Landfalling Atmospheric Rivers, the Sierra Barrier Jet and Extreme Daily Precipitation in Northern California's Upper Sacramento River Watershed

F. Martin Ralph[1], Jason M. Cordeira[2], Paul J. Neiman[3] and Mimi Hughes[3,4]

[1]*Center for Western Weather and Water Extremes, Scripps Institution of Oceanography, University of California San Diego, La Jolla, California*

[2]*Department of Atmospheric Science and Chemistry, Plymouth State University, Plymouth, NH*

[3]*Physical Sciences Division, NOAA/Earth System Research Laboratory, Boulder, Colorado*

[4]*Cooperative Institute for Research in the Environmental Sciences, University of Colorado, Boulder, Colorado*

Originally Submitted to J. Hydrometeor. September 2015

Resubmitted January 2016

Corresponding Author Address:
Jason M. Cordeira
17 High Street, MSC 48
Plymouth, NH 03264
Email: j_cordeira@plymouth.edu

Abstract

The Upper Sacramento River Watershed is vital to California's water supply, and is susceptible to major floods. Orographic precipitation in this complex terrain involves both atmospheric rivers (ARs) and the Sierra barrier jet (SBJ). The south-southeasterly SBJ induces orographic precipitation along south-facing slopes in the Mt. Shasta–Trinity Alps, whereas landfalling ARs ascend up and over the statically stable SBJ and induce orographic precipitation along west-facing slopes in the Northern Sierra Nevada. This paper explores the occurrence of extreme daily precipitation (EDP) in this region in association with landfalling ARs and the SBJ.

The 50 wettest days (i.e., days with EDP) for water years (WY) 2002–2011 based on the average of daily precipitation from eight rain gauges known as the "Northern Sierra 8-Station Index (NS8I)" are compared to dates from an SSM/I satellite-based landfalling AR-detection method and dates with SBJ events identified from nearby wind profiler data. These 50 days with EDP accounted for 20% of all precipitation during the 10-WY period, or five days with EDP per year on average account for one-fifth of WY precipitation. In summary, 46 of 50 (92%) of days with EDP are associated with landfalling ARs on either the day before or the day of precipitation, whereas 45 of 50 (90%) days with EDP are associated with SBJ conditions on the day of EDP. Forty-one of 50 (82%) days with EDP are associated with both a landfalling AR and an SBJ. The top-10 days with EDP were all associated with both a landfalling AR and an SBJ.

1. Introduction

The availability and management of water supply in California's North Central Valley (CV) along the Upper Sacramento River is strongly influenced by variability in cool-season precipitation, snowpack, and streamflow in the Northern Sierra Nevada and Mt. Shasta–Trinity Alps regions. The California Department of Water Resources (DWR), and other water managers who seek to gauge water supply, closely monitor the precipitation in this region using daily precipitation totals averaged across eight sites known as the Northern Sierra 8-station Index (NS8I; Fig. 1). Numerous studies suggest that a majority of cool-season precipitation in this region occurs in conjunction with winter storms and their interaction with the complex topography in association with landfalling atmospheric rivers (ARs) and terrain-locked Sierra barrier jets (SBJs; e.g., Dettinger 2004; Galewsky and Sobel 2005; Ralph et al. 2006, 2011, 2013a,b; Kim and Kang 2007; Reeves et al. 2008; Guan et al. 2010; Lundquist et al. 2010; Smith et al. 2010; Neiman et al. 2008b, 2010, 2013, 2014; Dettinger et al. 2011; Kim et al. 2012; White et al. 2015). The overarching objective of this study is to collectively identify what fraction of days with extreme daily precipitation (EDP) in the NS8I occurs in association with ARs and SBJs.

Atmospheric rivers are long (1000s km) and narrow (~500 km) regions of enhanced integrated water vapor (IWV) and integrated water vapor transport (IVT) located in the warm sector of transient midlatitude cyclones (e.g., Zhu and Newell 1998; Ralph et al. 2004, 2006; Neiman et al. 2008a,b). ARs typically represent regions of lower-tropospheric water vapor flux along a pre-cold-frontal low-level jet (e.g., Ralph et al. 2004). SBJs are a mountain-parallel core of locally strong winds composed primarily of ageostrophic flow at ~1 km AGL (Parish 1982). The SBJ forms in response to the deceleration of stably stratified westerly flow as it approaches

the west slope of the Sierra Nevada. This deceleration of westerly flow leads to a lower-tropospheric acceleration of a southerly ageostrophic wind and a core of Sierra-parallel (~160°) winds along the windward slope beneath Sierra crest level (~3 km).

Individual case studies and composite studies of EDP across northern California have identified that both landfalling ARs and south-southeasterly SBJs are associated with heavy orographic precipitation along the west slope of the Northern Sierra Nevada and south slope of the Mt. Shasta–Trinity Alps, respectively (e.g., Neiman et al. 2010, 2013, 2014; Ralph et al. 2011; Ralph and Dettinger 2012; Kingsmill et al. 2013; White et al. 2015). A majority (75%) of water vapor flux within ARs located over the eastern North Pacific occurs within the lowest 2.25 km of the troposphere (Ralph et al. 2006), whereas a prominent peak in water vapor flux along the SBJ in the northern CV occurs at ~1.5 km (Neiman et al. 2013). In environments often characterized by moist neutral static stability (Neiman et al. 2008a), heavy orographic precipitation often results in regions where water vapor flux along ARs and SBJs intersect mountainous terrain. The so-called "upslope IWV flux" explains up to 70% of the variance in total precipitation that results from forced saturated ascent along ARs (Ralph et al. 2006) and explains >80% of the variance in hourly precipitation rate that occurs in association with forced saturated ascent along SBJs (Neiman et al. 2013).

The studies by Neiman et al. (2013, 2014) and Kingsmill et al. (2013) identify that ARs are capable of transporting lower-tropospheric water vapor into California's North CV through openings in terrain over north-coastal California known as the Petaluma Gap and the San Francisco Bay Gap (Fig. 1). Once in the CV, the water vapor may either ascend and produce orographic enhanced precipitation above SBJ altitudes along the west slope of the Northern Sierra Nevada or be carried northward at low altitudes (~1–2 km) along the SBJ to later ascend

and produce orographic enhanced precipitation along the south slope of the Mt. Shasta–Trinity Alps (see Fig. 13 from Neiman et al. 2013). The stations that comprise the NS8I are therefore ideally located along the slopes of these topographic features (Fig. 1) in order to adequately investigate what fraction of days with EDP in the NS8I occurs in association with ARs and SBJs. Based on the results of Neiman et al. (2013, 2014) and Kingsmill et al. (2013), we hypothesize that a large majority of EDP in the NS8I occurs in conjunction with both landfalling ARs and the SBJ.

The proposed hypothesis is tested through investigation of the 50 largest daily precipitation totals measured by the NS8I over a ten water-year (WY) period from WY 2002 through WY 2011 (e.g., WY 2002 is 1 October 2001–30 September 2002). Section 2 describes the data and methodology, whereas section 3 presents event statistics and composite analyses. A summarizing discussion is found in section 4.

2. Data and Methods

The EDP across the Northern Sierra Nevada and Mt. Shasta–Trinity Alps region is identified from daily precipitation totals averaged across the eight gauges comprising the NS8I. The NS8I is available from the State of California Department of Water Resources–California Data Exchange Center online at http://cdec.water.ca.gov/cdecapp/precipapp/get8SIPrecipIndex.action. The EDP is defined in this study as the 50 days with the largest daily precipitation totals during WY 2002–2011, representing a manageable number of days to evaluate and the wettest ~1.37% of daily precipitation totals during this period.

Landfalling ARs are identified following the methodology used to create a catalog of ARs described by Neiman et al. (2008b) that uses a Special Sensor Microwave Imager (SSM/I;

Hollinger et al. 1990) satellite-based IWV detection method (Wentz 1995) that was first used by Ralph et al. (2004). This methodology includes a subjective identification of ARs using objective criteria that require narrow plumes of IWV with values >2 cm that are >2000 km long and <1000 km wide to intersect the U.S. West Coast between 32.5°N and 41.0°N (Fig. 2a; see Neiman et al. 2008b). The presence of an AR meeting these criteria is noted on either the day of EDP or the day prior in order to account for the low temporal resolution (twice-daily) observations from the SSM/I instrument. The SBJs are identified from data collected from a 915-MHz radar wind profiler (Carter et al. 1995) located at Chico (CCO), CA that was deployed by the NOAA Earth Systems Research Laboratory as part of the Hydrometeorology Testbed-West (Ralph et al. 2013). The SBJs are identified using the Neiman et al. (2010) methodology that requires (1) A Sierra-parallel (160°) wind speed, V_s, >12 m s^{-1} below 3 km, (2) a maximum V_s located ≥200 m AGL, and (3) a V_s that decreases by >2 m s^{-1} between the level of maximum V_s and 3 km (Fig. 2b). Presence of an SBJ meeting these criteria is noted on the day of EDP.

Composite analyses are constructed from the North American Regional Reanalysis (NARR; Mesinger et al. 2006) for the 50 days with EDP in order to illustrate water vapor flux along landfalling ARs and south-southeasterly SBJs. The NARR contains data with 32-km horizontal grid spacing on 45 vertical levels that are available at 3-h intervals; however, only the 0000 UTC reanalysis periods for the day with EDP are used in this study. Although the grid spacing of the NARR is sufficient for synoptic–mesoscale analysis of ARs and the SBJ (e.g., Neiman et al. 2014), it has a known positive elevation bias in the altitude of wind speed maxima along the SBJ and a negative magnitude bias in water vapor flux along the SBJ as compared to higher resolution downscaled simulations owing to a coarse representation of terrain across northern California (Hughes et al. 2012).

3. Results

a. Event Statistics

The 50 EDP totals identified in the NS8I ranged from 43 mm to 103 mm, contained a mean value of 55 mm, and contributed to ~2–7% of their respective total water–year precipitation (Table 1). The 50 days with EDP (1.37% of all days) accounted for 20% of all observed precipitation during the 10-WY period. In order words, five days with EDP per year on average account for one-fifth of WY precipitation in this region. The 50 EDP totals were part of several multi-day precipitation events: 24 of 50 (45%) days with EDP occurred on consecutive days or at least twice on three consecutive days. The mean value of the highest 72-h precipitation totals that included the 24-h period with EDP from individual stations that comprise the NS8I was 210 mm; the highest 72-h precipitation total at any one station within the NS8I was 369 mm. The 72-h precipitation totals on 18 of 50 days are "R-CAT 1" precipitation events (200–300 mm), whereas four of 50 days are "R-CAT 2" precipitation events (300–400 mm) according to the methodology of Ralph and Dettinger (2012). Forty-eight of the 50 days with EDP occurred during the October–March cool season, which is consistent with occurrences of heavy precipitation caused by landfalling ARs identified by Ralph and Dettinger (2012).

Forty-six of 50 (92%) days with EDP occur on the day after or day of a landfalling AR, whereas 45 of 50 (90%) days with EDP occur on days with an SBJ. Forty-one of 50 (82%) days with EDP occur in association with both landfalling ARs and SBJ, and all 50 days with EDP occur in association with either a landfalling AR or SBJ. The 10 days with the largest EDP totals all occur in association with both a landfalling AR and SBJ conditions. Section 3b explores the synoptic and mesoscale processes associated with landfalling ARs and the SBJ related to EDP.

b. Composite Analysis

Composite analysis of the IWV, IVT, sea-level pressure, and 900-hPa winds (Figs. 3 a–b) illustrates that the 50 days with EDP occurred in conjunction with an occluded low-pressure center (992 hPa) located over the Northeast Pacific near 48°N, 133°W. The warm sector of this occluded cyclone contained broad westerly to southwesterly 900-hPa flow >10 m s^{-1} in an environment with IWV values >2.4 cm and IVT magnitudes >450 kg m^{-1} s^{-1} that spans from near Hawaii (not shown) to the central CA coast (Fig. 3a). The composite IWV and IVT structures suggest that this feature is an AR with a length scale of >2000 km and a width of ~1500 km. Note that inspection of the IWV and IVT structure from individual cases highlight a more characteristic width of <1000 km; thus the large composite width is the effect of averaging over many events with differing spatial structures. The IWV along this composite AR is transported to the northeast along a streamline oriented ~230° through the San Francisco Bay Gap (Fig. 1) and into the Northern CV (Fig. 3b). The SBJ is observed in this composite analysis as a backing of ~7.5 m s^{-1} 900-hPa winds to south-southeast (~160°) over and within the Northern CV. For comparison purposes, the top-10 days with EDP are associated with a stronger occluded low pressure system (982 hPa) containing more intense AR conditions with IWV values >3.0 cm and IVT magnitudes >650 kg m^{-1} s^{-1} (Fig. 3c) and more intense SBJ conditions with 900-hPa south-southeasterly winds >10 m s^{-1} (Fig. 3d).

An AR-parallel composite cross section analysis that spans the Northeast Pacific, Coastal Range, Northern CV, and Northern Sierra Nevada illustrates that the 50 days with EDP occur in association with a south-southeast total wind that is ~7.5 m s^{-1} along an SBJ near 1 km over the Northern CV and a west-southwest total wind that is ~7.5–10 m s^{-1} farther west along the AR

near 0.50 km that increases to >12.5 m s^{-1} over the Northern Sierra Nevada above 3 km (Fig. 4a). Water vapor flux along the SBJ (i.e., total water vapor flux projected onto 160°) peaks near 1 km with a magnitude of >20 kg m^{-1} s^{-1} along the west slope of the Northern Sierra Nevada, whereas water vapor flux along the AR (i.e., total water vapor flux projected onto 230°) peaks below 1 km over the Northeast Pacific and again above the crest of the Northern Sierra Nevada above 3 km with magnitudes >20 kg m^{-1} s^{-1}. A majority of the water vapor flux along both the AR and the SBJ occurs below the ~2.5-km freezing level that is located above crest-level of the Northern Sierra Nevada, which suggests that any precipitation in the presence of orographic ascent would fall in liquid form. The decrease in water vapor flux along the AR from the Northeast Pacific into the Northern CV is consistent with the observed west-to-east decrease in IVT along the AR in Fig. 3a, whereas the maximum in water vapor flux above the crest of the Northern Sierra occurs in conjunction with the increase in total wind speed. The increase in altitude of the water vapor flux maximum along the AR from below 1 km over the Northeast Pacific to above 3 km over the Northern Sierra Nevada is consistent with detailed experimental observations of water vapor flux rising over the SBJ (Kingsmill et al. 2013; Neiman et al. 2014). For comparison purposes, the top-10 days with EDP are associated with a similar horizontal and vertical structure of water vapor flux along the AR and SBJ with magnitudes that are >30 kg m^{-1} s^{-1} (Fig. 4b). Note that a maximum in water vapor flux from 160° also occurs along a lower-tropospheric coastal barrier jet that could influence orographic precipitation gradients along the Coastal Range (e.g., Lundquist et al. 2010); this topic is beyond the scope of the current investigation.

4. Discussion and Summary

This study investigated the 50 wettest days across the Upper Sacramento River watershed and their association with landfalling ARs and SBJs during WY 2002–2011. The 50 wettest days, referred to as days with EDP, are derived from the NS8I that is used by DWR and other water managers to gauge water supply in the Upper Sacramento River watershed region. A large majority of the 50 days with EDP occurred on the day of or the day after a landfalling AR (92%), on the day of an SBJ (90%), or both (82%). All 50 days with EDP occurred in association with either an AR or SBJ. The top-10 days with EDP all occurred in association with both a landfalling AR and a SBJ.

Composite analysis of the 50 days with EDP illustrates that extreme precipitation across the Northern Sierra Nevada and Mt. Shasta–Trinity Alps region is largely influenced by a west-southwesterly water vapor flux along a landfalling AR that increases in altitude from below 1 km over the Northeast Pacific to ~3 km over the Northern Sierra Nevada and is locally influenced by a low-altitude south-southeasterly water vapor flux along an SBJ at ~1 km. The horizontal and vertical structure of water vapor fluxes along landfalling ARs and SBJs on days with EDP in the NS8I complement the results from case studies and similar investigations that describe the relationships among landfalling ARs, SBJs, and precipitation distributions over the Northern Sierra and Mt. Shasta–Trinity Alps regions by Kingsmill et al. (2013) and Neiman et al. (2010, 2013, 2014). The stronger values of water vapor fluxes along landfalling ARs and SBJs on the top-10 days with EDP also complement results from Ralph et al. (2006) and Neiman et al. (2010, 2013) that indicate stronger values of water vapor flux along landfalling ARs and SBJs produce more intense precipitation and higher precipitation totals.

The results presented in section 3 indicate that landfalling ARs and SBJs are important synoptic and mesoscale processes, respectively, responsible for producing EDP in the NS8I;

however, these results do not necessarily indicate which process is more important. For example, the data in Table 1 can be used to identify that the NS8I on days with EDP is not statistically (according to a student's t-test) higher or lower on days with ARs versus days without ARs, nor is it statistically higher or lower on days with SBJs versus days without SBJs, and nor is it statistically higher or lower on days with both an AR and SBJ versus days without both. The aggregation of the eight stations within the NS8I does not allow for separation of the two processes. Bifurcation of the eight stations into two groups (e.g., the two stations along the south-facing slopes of the Mt. Shasta–Trinity Alps region and the six remaining stations along the west-facing slopes of the Northern Sierra Nevada) allows for insight into the relative importance of the SBJ and AR on EDP. For example, the average precipitation of the six easterly (two northerly) stations on days with EDP is not significantly higher (lower) on days with ARs versus days without ARs; however, the average precipitation at the two northerly stations is significantly higher on days with EDP that occur on SBJ days as compared to non-SBJ days. These results suggest that EDP across the more northern region of the Upper Sacramento River watershed in proximity to the Mt. Shasta–Trinity Alps region can be significantly influenced by the presence of an SBJ. The EDP in this region in association with the SBJ can therefore have a large impact on water resource management, for example, at California's largest reservoir at Shasta Lake behind Shasta Dam (Fig. 1).

The findings presented in this paper suggest that accurate forecasts of EDP in the Upper Sacramento River watershed are influenced in part by how well prediction systems resolve both synoptic-scale and mesoscale processes over northern California in conjunction with landfalling ARs and the SBJ. For example, the terrain-induced positive elevation bias in the altitude of maximum wind speed along the SBJ and negative magnitude bias in water vapor flux along the

SBJ identified by Hughes et al. (2012) in NARR analyses as compared to higher resolution downscaled simulations indicates that a weather prediction model capable of accurately resolving the terrain across CA and attendant synoptic-influenced and terrain-induced mesoscale circulations will likely perform better at forecasting EDP than a lower resolution model. Given the complex nature of the terrain and terrain-induced mesoscale circulations, it is recommended that future forecast system enhancements include both detailed monitoring and prediction of landfalling ARs and the SBJ in this region. Given the established linkages between ARs and SBJs (e.g., Kingsmill et al. 2013; Neiman et al. 2013, 2014), between ARs and streamflow (e.g., Neiman et al. 2011), and between SBJs and streamflow (e.g., Neiman et al. 2014), this effort would enable short lead time refinements to reservoir operations under potential flood conditions, as documented during the Howard Hanson Dam flood-risk crisis in Washington (White et al. 2012), and could be achieved as an expansion of the "Enhanced Flood Response and Emergency Preparedness" observing network recently installed in California (White et al. 2013, Ralph et al. 2014).

5. Acknowledgments

This research was supported by funding provided by award #4600010378 through the California Department of Water Resources. Comments by three anonymous reviewers greatly improved the quality of this manuscript.

6. References

Carter, D. A., K. S. Gage, W. L. Ecklund, W. M. Angevine, P. E. Johnston, A. C. Riddle, J. S. Wilson, and C. R. Williams, 1995: Developments in UHF lower tropospheric wind

profiling at NOAA's Aeronomy Laboratory. *Radio Sci.,* **30,** 977–1001, doi:10.1029/95RS00649.

Dettinger, M. D., 2004: Fifty-two years of ''pineapple-express'' storms across the West Coast of North America. U.S. Geo- logical Survey, Scripps Institution of Oceanography for the California Energy Commission, PIER Project Rep. CEC-500-2005-004, 20 pp. [Available online at http://www.energy.ca.gov/2005publications/CEC-500-2005-004/CEC-500-2005-004.PDF.]

Dettinger, M. D., F. M. Ralph, T. Das, P. J. Neiman, and D. Cayan, 2011: Atmospheric rivers, floods, and the water resources of California. *Water,* **3,** 455–478, doi:10.3390/w3020445.

Galewsky, J., and A. Sobel, 2005: Moist dynamics and orographic precipitation in northern and central California during the New Year's Flood of 1997. *Mon. Wea. Rev.,* **133,** 1594–1612, doi:10.1175/MWR2943.1.

Guan, B., N. Molotch, D. Waliser, E. Fetzer, and P. J. Neiman, 2010: Extreme snowfall events linked to atmospheric rivers and surface air temperature via satellite measurements. *Geophys. Res. Lett.,* **37,** L20401, doi:10.1029/2010GL044696.

Hollinger, J. P., J. L. Peirce, and G. A. Poe, 1990: SSM/I instrument evaluation. *IEEE Trans. Geosci. Remote Sens.,* **28,** 781–790, doi:10.1109/36.58964.

Hughes, M., P. J. Neiman, E. Sukovich, and F. M. Ralph, 2012: Representation of the Sierra Barrier Jet in 11 years of a high-resolution dynamical reanalysis downscaling. *J. Geophys. Res.,* **117,** D18116, doi:10.1029/2012JD017869.

Kim, J., and H.-S. Kang, 2007: The impact of the Sierra Nevada on low-level winds and water vapor transport. *J. Hydrometeor.,* **8,** 790–804, doi:10.1175/JHM599.1.

Kim. J., D. E. Waliser, P. J. Neiman, B. Guan, J.-M. Ryoo, and G. A. Wick, 2012: Effects of

atmospheric river landfalls on the cold season precipitation in California. *Climate Dyn.,* **38,** 411– 429, doi:10.1007/s00382-010-0972-2.

Kingsmill, D. E., P. J. Neiman, B. J. Moore, M. Hughes, S. E. Yuter, and F. M. Ralph, 2013: Kinematic and thermodynamic structures of Sierra barrier jets and overrunning atmospheric rivers during a land-falling winter storm in northern California. *Mon. Wea. Rev.,* **141,** 2015–2036, doi:10.1175/ MWR-D-12-00277.1.

Lundquist, J. D., J. R. Minder, P. J. Neiman, and E. M. Sukovich, 2010: Relationships between barrier jet heights, precipitation distributions, and streamflow in the northern Sierra Nevada. *J. Hydrometeor.,* **11,** 1141–1156, doi:10.1175/2010JHM1264.1.

Mesinger, F., and Coauthors, 2006: North American Regional Reanalysis. *Bull. Amer. Meteor. Soc.,* **87,** 343–360, doi:10.1175/ BAMS-87-3-343.

Neiman, P. J., F. M. Ralph, G. A. Wick, Y.-H. Kuo, T.-K. Wee, Z. Ma, G. H. Taylor, and M. D. Dettinger, 2008a: Diagnosis of an intense atmospheric river impacting the Pacific Northwest: Storm summary and offshore vertical structure observed with COSMIC satellite retrievals. *Mon. Wea. Rev.,* **136,** 4398–4420, doi:10.1175/2008MWR2550.1.

Neiman, P. J., F. M. Ralph, G. A. Wick, J. Lundquist, and M. D. Dettinger, 2008b: Meteorological characteristics and overland precipitation impacts of atmospheric rivers affecting the West Coast of North America based on eight years of SSM/I satellite observations. *J. Hydrometeor.,* **9,** 22–47, doi:10.1175/2007JHM855.1.

Neiman, P. J., E. M. Sukovich, F. M. Ralph, and M. Hughes, 2010: A seven-year wind profiler-based climatology of the windward barrier jet along California's northern Sierra Nevada. *Mon. Wea. Rev.,* **138,** 1206–1233, doi:10.1175/2009MWR3170.1.

Neiman, P. J., L. J. Schick, F. M. Ralph, M. Hughes, and G. A. Wick, 2011: Flooding in western

Washington: The connection to atmospheric rivers. *J. Hydrometeor*. 12, 1337–1358.

Neiman, P. J., M. Hughes, B. J. Moore, F. M. Ralph, and E. S. Sukovich, 2013: Sierra barrier jets, atmospheric rivers, and precipitation characteristics in northern California: A composite perspective based on a network of wind profilers. *Mon. Wea. Rev.,* **141,** 4211–4233, doi:10.1175/MWR-D-13-00112.1.

Neiman, P. J., F. M. Ralph, B. J. Moore, and B. J. Zamora, 2014: The regional influence of an intense Sierra barrier jet and landfalling atmospheric river on orographic precipitation in Northern California: A case study. *J. Hydrometor.,* **15,** 1419–1439, doi:10.1175/JHM-D-13-0183.1.

Parish, T. R., 1982: Barrier winds along the Sierra Nevada mountains. *J. Appl. Meteor.,* **21,** 925–930.

Ralph, F. M., and M. D. Dettinger, 2012: Historical and national perspectives on extreme West Coast precipitation associated with atmospheric rivers during December 2010. *Bull. Amer. Meteor. Soc.,* **93,** 783–790, doi:10.1175/BAMS-D-11-00188.1.

Ralph, F. M., P. J. Neiman, and G. A. Wick, 2004: Satellite and CALJET aircraft observations of atmospheric rivers over the eastern North Pacific Ocean during the winter of 1997/98. *Mon. Wea. Rev.,* **132,** 1721–1745, doi:10.1175/1520-0493(2004)132,1721:SACAOO.2.0.CO;2.

Ralph, F. M., P. J. Neiman, G. A. Wick, S. I. Gutman, M. D. Dettinger, D. R. Cayan, and A. B. White, 2006: Flooding on California's Russian River: The role of atmospheric rivers. *Geophys. Res. Lett.,* **33,** L13801, doi:10.1029/2006GL026689.

Ralph, F. M., P. J. Neiman, G. N. Kiladis, K. Weickmann, and D. M. Reynolds, 2011: A multi-scale observational case study of a Pacific atmospheric river exhibiting tropical–

extratropical connections and a mesoscale frontal wave. *Mon. Wea. Rev.,* **139,** 1169–1189, doi:10.1175/2010MWR3596.1.

Ralph, F.M., J. Intrieri, D. Andra Jr., S. Boukabara, D. Bright, P. Davidson, B. Entwistle, J. Gaynor, S. Goodman, J. Gwo-Jiing, A. Harless, J. Huang, G. Jedlovec, J. Kain, S. Koch, B. Kuo, J. Levit, S.T. Murillo, L.P. Riishojgaard, T. Schneider, R. Schneider, T. Smith, and S. Weiss, 2013: The emergence of weather-focused testbeds linking research and forecasting operations. *Bull. Amer. Meteor. Soc.*, **94**, 1187-1210.

Ralph, F. M., M. Dettinger, A. White, D. Reynolds, D. Cayan, T. Schneider, R. Cifelli, K. Redmond, M. Anderson, F. Gherke, J. Jones, K. Mahoney, L. Johnson, S. Gutman, V. Chandrasekar, J. Lundquist, N.P. Molotch, L. Brekke, R. Pulwarty, J. Horel, L. Schick, A. Edman, P. Mote, J. Abatzoglou, R. Pierce and G. Wick, 2014: A vision for future observations for Western U.S. extreme precipitation and flooding– Special Issue of *J. Contemporary Water Resources Research and Education*, Universities Council for Water Resources, Issue 153, pp. 16-32.

Reeves, H. D., Y.-L. Lin, and R. Rotunno, 2008: Dynamic forcing and mesoscale variability of heavy precipitation events over the Sierra Nevada Mountains. *Mon. Wea. Rev.,* **136,** 62–77, doi:10.1175/2007MWR2164.1.

Smith, B. L., S. E. Yuter, P. J. Neiman, and D. E. Kingsmill, 2010: Water vapor fluxes and orographic precipitation over northern California associated with a land-falling atmospheric river. *Mon. Wea. Rev.,* **138,** 74–100, doi:10.1175/ 2009MWR2939.1.

Wentz, F. J., 1995: The intercomparison of 53 SSM/I water vapor algorithms. Remote Sensing Systems Tech. Rep. on WetNet Water Vapor Intercomparison Project (VIP), Santa Rosa, CA, 19 pp.

White, A. B., B. Colman, G. M. Carter, F. M. Ralph, R. S. Webb, D. G. Brandon, C. W. King, P. J. Neiman, D. J. Gottas, I. Jankov, K. F. Brill, Y. Zhu, K. Cook, H. E. Buehner, H. Opitz, D. W. Reynolds, L. J. Schick, 2012: NOAA's Rapid Response to the Howard A. Hanson Dam Flood Risk Management Crisis. *Bull. Amer. Meteorol. Soc.,* **93**, 189-207, doi: 10.1175/BAMS-D-11-00103.1.

White, A.B., M.L. Anderson, M.D. Dettinger, F.M. Ralph, A. Hinojosa, D.R. Cayan, R.K. Hartman, D.W. Reynolds, L.E. Johnson, T.L. Schneider, R. Cifelli, Z. Toth, S.I. Gutman, C.W. King, F. Gehrke, P.E. Johnston, C. Walls, D. Mann, D.J. Gottas and T. Coleman, 2013: A 21st century California observing network for monitoring extreme weather events. *J. Atmos. Ocean. Technol.*, **30**, 1585-1603.

White, A.B., P.J. Neiman, J.M. Creamean, T. Coleman, F.M. Ralph and K.A. Prather, 2015: The Impacts of California's San Francisco Bay Area Gap on Precipitation Observed in the Sierra Nevada during HMT and CalWater. *J. Hydrometeor*, **16**, 1048–1069.

Zhu, Y., and R. E. Newell, 1998: A proposed algorithm for moisture fluxes from atmospheric rivers. *Mon. Wea. Rev.,* **126,** 725–735, doi:10.1175/1520-0493(1998)126,0725:APAFMF.2.0.CO;2.

7. Tables

Table 1. Dates and characteristics of the 50 days with EDP within the NS8I. Characteristics include the 24-h precipitation, 24-h precipitation as a percentage of water-year precipitation, AR landfall on the day of EDP or the day prior, SBJ on the day of EDP, the maximum 72-h precipitation at any of the eight stations, the 72-h precipitation as a % of water-year precipitation, and the R-CAT designation following the methodology of Ralph and Dettinger (2012). The 10 wettest days with EDP are indicated with an asterisk.

Date	**NS8I 24-h precip**	**24-h precip as % WY**	**AR?**	**SBJ?**	**Max 72-h station precip**	**R-Cat of Max 72-h precip**
YYYYMMDD	[mm]	[%]	[Y or N]	[Y or N]	[mm]	[0 … 4]
20011124	46	3.8	Y	Y	120	0
20011202	50	4.1	Y	Y	180	0
20020102	44	3.6	Y	Y	105	0
20021108*	76	5.0	Y	Y	180	0
20021213	59	3.9	Y	Y	369	2
20021214*	103	6.8	Y	Y	369	2
20021215	55	3.6	N	Y	369	2
20021216*	65	4.3	Y	Y	349	2
20021227	43	2.9	Y	Y	228	1
20021228	54	3.6	Y	Y	228	1
20030314	47	3.1	Y	Y	154	0
20030315	58	3.8	Y	Y	154	0
20031206	48	4.0	Y	Y	177	0
20031224	50	4.2	Y	Y	128	0
20031229	44	3.7	Y	Y	172	0
20040101	43	3.6	Y	Y	122	0
20040216	43	3.6	Y	Y	281	1
20040217*	72	6.0	Y	Y	281	1
20040226	53	4.4	Y	Y	176	0
20041207	46	3.1	Y	Y	245	1
20041208*	71	4.8	Y	Y	245	1
20041230	45	3.1	N	Y	196	0
20050518	48	3.3	Y	Y	178	0
20051201*	66	3.2	Y	Y	218	1
20051202	43	2.1	Y	Y	189	0
20051221	48	2.4	Y	N	260	1
20051222	57	2.8	Y	Y	260	1
20051226	44	2.2	Y	Y	173	0
20051228*	63	3.1	Y	Y	243	1
20051230	49	2.4	Y	Y	299	1
20051231*	99	4.8	Y	Y	299	1
20060227*	66	3.2	Y	Y	184	0
20060228	59	2.9	Y	N	184	0
20060403	49	2.4	Y	Y	162	0
20070210	51	5.4	Y	Y	262	1
20080104	50	5.4	Y	Y	160	0
20080105	46	5.0	Y	N	160	0
20081101	50	4.1	N	Y	157	0
20090223	60	4.8	Y	Y	181	0
20090302	59	4.8	Y	Y	194	0
20090303	47	3.8	Y	N	194	0
20091014	55	3.9	Y	Y	150	0
20100118	48	3.4	Y	Y	204	1
20100119	47	3.3	Y	Y	204	1
20101024*	97	5.1	Y	Y	269	1
20101218	57	3.0	Y	Y	226	1
20101219	44	2.3	Y	N	226	1
20110316	46	2.4	Y	Y	139	0
20110319	50	2.6	N	Y	141	0
20110320	45	2.4	Y	Y	141	0
Top 10 counts			10/10	10/10		
Top 50 counts			46/50	45/50		

8. Figure Captions

Fig. 1. The locations, IDs, and altitude (m MSL; inset table) of the eight stations that comprise the Northern Sierra 8-Station Index (yellow triangles) atop terrain elevation (m; shaded according to scale) and an outline of the Sacramento River watershed (blue shade) and its tributaries (blue lines). The location of the Chico (CCO), CA wind profiler is indicated by the white "+" symbol.

Fig. 2: (a) Annotated SSM/I satellite-based IWV (cm; shaded) on 16 February 2004 that illustrates method used to detect the presence of a landfalling AR in each of the 50 days with EDP. Only ARs making landfall in California are counted (i.e., between 32.5°N and 41°N as in the Neiman et al. 2008b AR catalog). (b) Annotated time–height section adapted from Neiman et al. (2010) of hourly averaged wind profiles (Flag = 25 m s^{-1}; Barb = 5 m s^{-1}; Half barb = 2.5 m s^{-1}) and barrier-parallel isotachs (m s^{-1}; directed from 160°) at Chico, CA on 25 Feb 2004 that illustrates method used to detect the presence of an SBJ.

Fig. 3. NARR composite analyses of the (a–b) 50 days and (c–d) top-10 days with EDP that illustrate IWV (cm; shaded according to scale), sea-level pressure (gray contours every 2 hPa), IVT magnitude (dashed contours every 100 kg m^{-1} s^{-1} beginning at 250 kg m^{-1} s^{-1}), and 900-hPa total wind (m s^{-1}; reference vector in upper right of panel). Panels (b) and (d) as in (a) and (c), except for a zoomed-in area over the Northern CV. The red "L" notes the composite location and intensity of the sea level pressure minimum. The purple cross section line is for Fig. 4. The purple square in panels (a) and (c) are the boundaries for panels (b) and (d).

Fig. 4. Composite cross section along an AR-parellel line from 37.5°N, 124°W to 40°N, 120°W (shown in Fig. 3) of the (a) 50 days and (b) top-10 days with EDP that illustrates SBJ water vapor (WV) flux (kg m^{-1} s^{-1}; shaded according to scale), AR WV flux (contoured every 5 kg m^{-1} s^{-1} beginning at 5 kg m^{-1} s^{-1}) and total wind barbs (as in Fig. 2b). The SBJ WV flux is projection of total WV flux along 160°, whereas AR WV flux is projection of total WV flux along 230°.

9. Figures

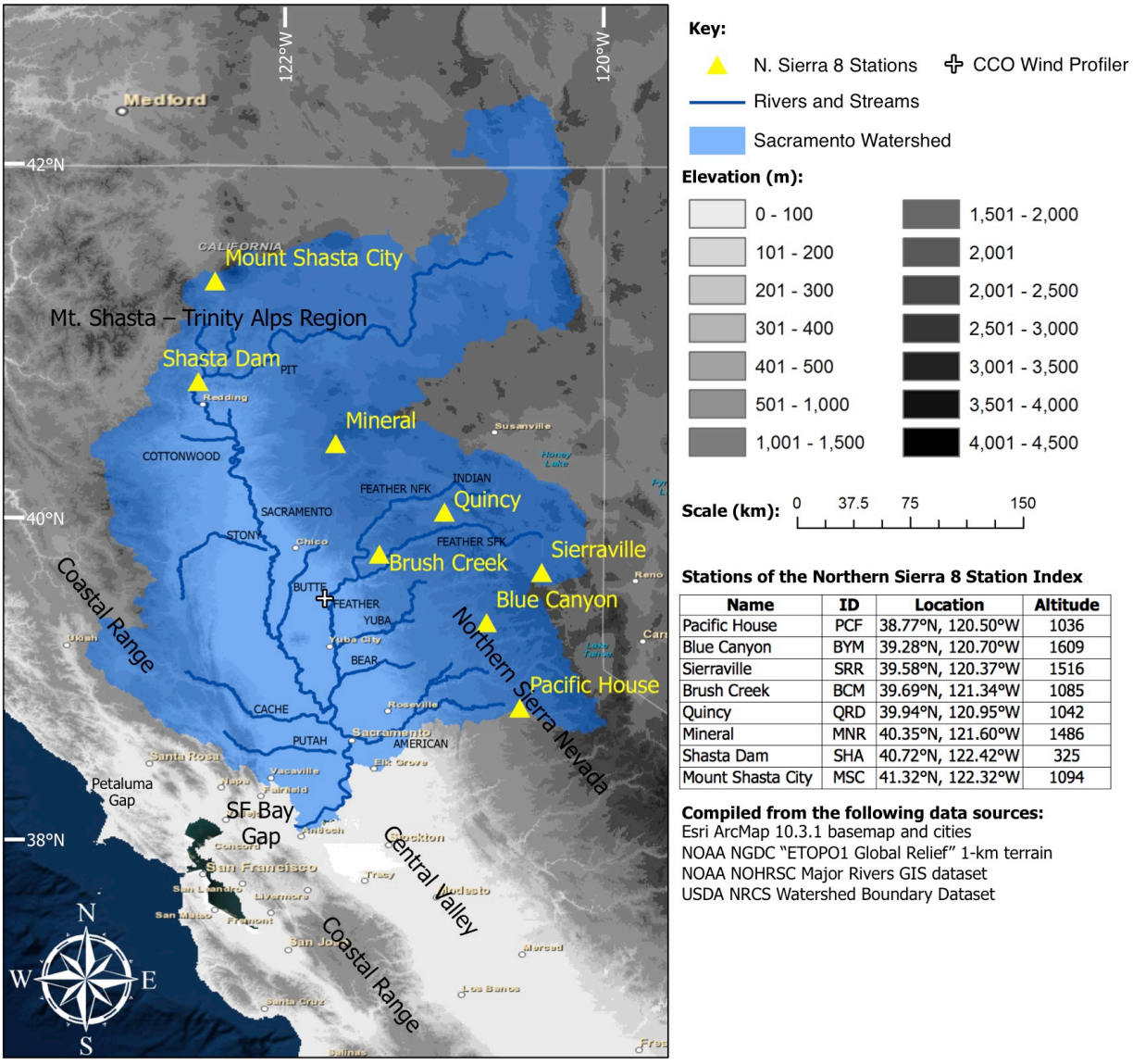

Stations of the Northern Sierra 8 Station Index

Name	ID	Location	Altitude
Pacific House	PCF	38.77°N, 120.50°W	1036
Blue Canyon	BYM	39.28°N, 120.70°W	1609
Sierraville	SRR	39.58°N, 120.37°W	1516
Brush Creek	BCM	39.69°N, 121.34°W	1085
Quincy	QRD	39.94°N, 120.95°W	1042
Mineral	MNR	40.35°N, 121.60°W	1486
Shasta Dam	SHA	40.72°N, 122.42°W	325
Mount Shasta City	MSC	41.32°N, 122.32°W	1094

Compiled from the following data sources:
Esri ArcMap 10.3.1 basemap and cities
NOAA NGDC "ETOPO1 Global Relief" 1-km terrain
NOAA NOHRSC Major Rivers GIS dataset
USDA NRCS Watershed Boundary Dataset

Fig. 1. The locations, IDs, and altitude (m MSL; inset table) of the eight stations that comprise the Northern Sierra 8-Station Index (yellow triangles) atop terrain elevation (m; shaded according to scale) and an outline of the Sacramento River watershed (blue shade) and its tributaries (blue lines). The location of the Chico (CCO), CA wind profiler is indicated by the white "+" symbol.

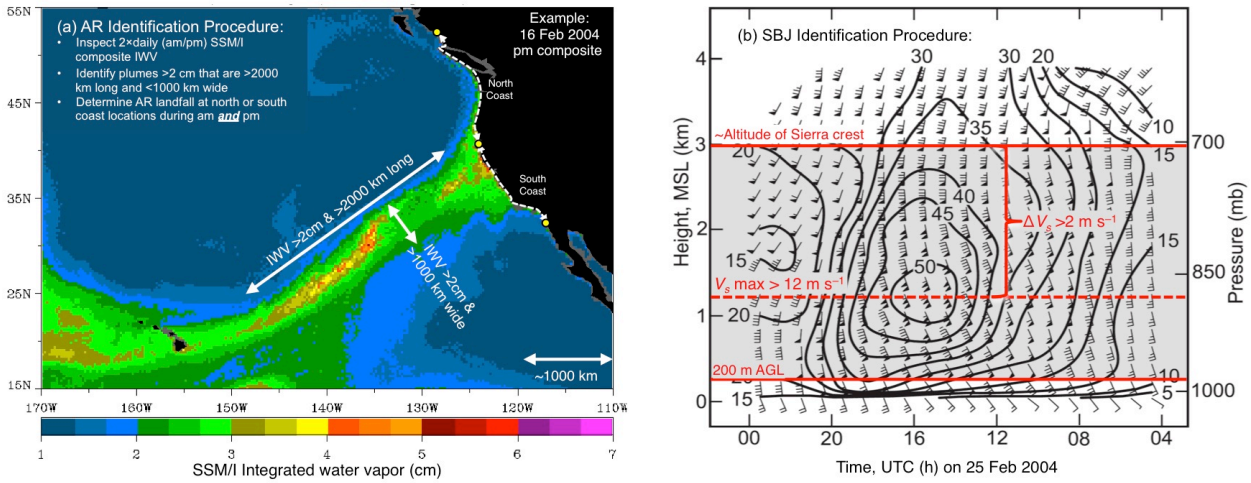

Fig. 2: (a) Annotated SSM/I satellite-based IWV (cm; shaded) on 16 February 2004 that illustrates method used to detect the presence of a landfalling AR in each of the 50 days with EDP. Only ARs making landfall in California are counted (i.e., between 32.5°N and 41°N as in the Neiman et al. 2008b AR catalog). (b) Annotated time–height section adapted from Neiman et al. (2010) of hourly averaged wind profiles (Flag = 25 m s^{-1}; Barb = 5 m s^{-1}; Half barb = 2.5 m s^{-1}) and barrier-parallel isotachs (m s^{-1}; directed from 160°) at Chico, CA on 25 Feb 2004 that illustrates method used to detect the presence of an SBJ.

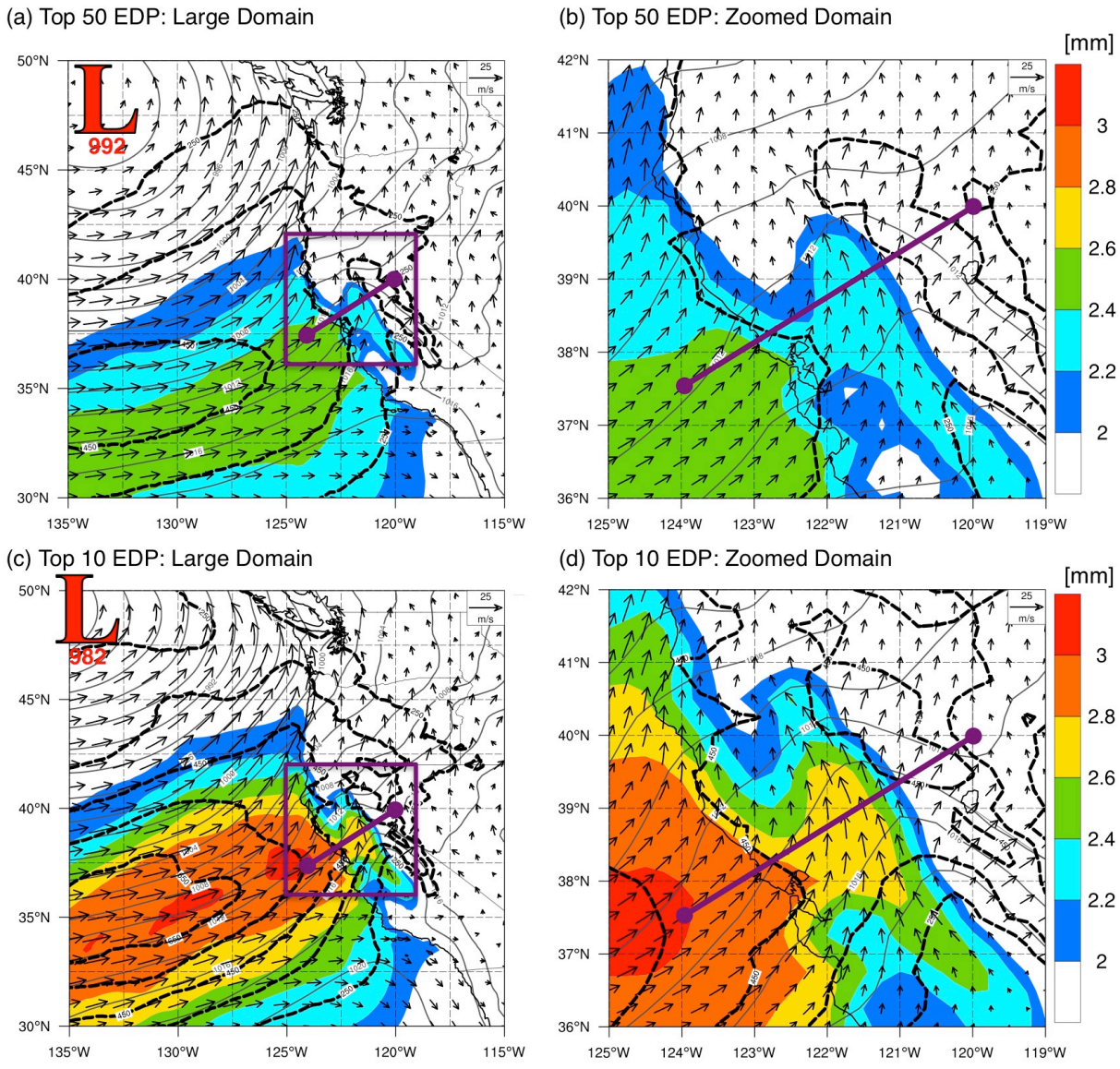

Fig. 3. NARR composite analyses of the (a–b) 50 days and (c–d) top-10 days with EDP that illustrate IWV (cm; shaded according to scale), sea-level pressure (gray contours every 2 hPa), IVT magnitude (dashed contours every 100 kg m^{-1} s^{-1} beginning at 250 kg m^{-1} s^{-1}), and 900-hPa total wind (m s^{-1}; reference vector in upper right of panel). Panels (b) and (d) as in (a) and (c), except for a zoomed-in area over the Northern CV. The red "L" notes the composite location and intensity of the sea level pressure minimum. The purple cross section line is for Fig. 4. The purple square in panels (a) and (c) are the boundaries for panels (b) and (d).

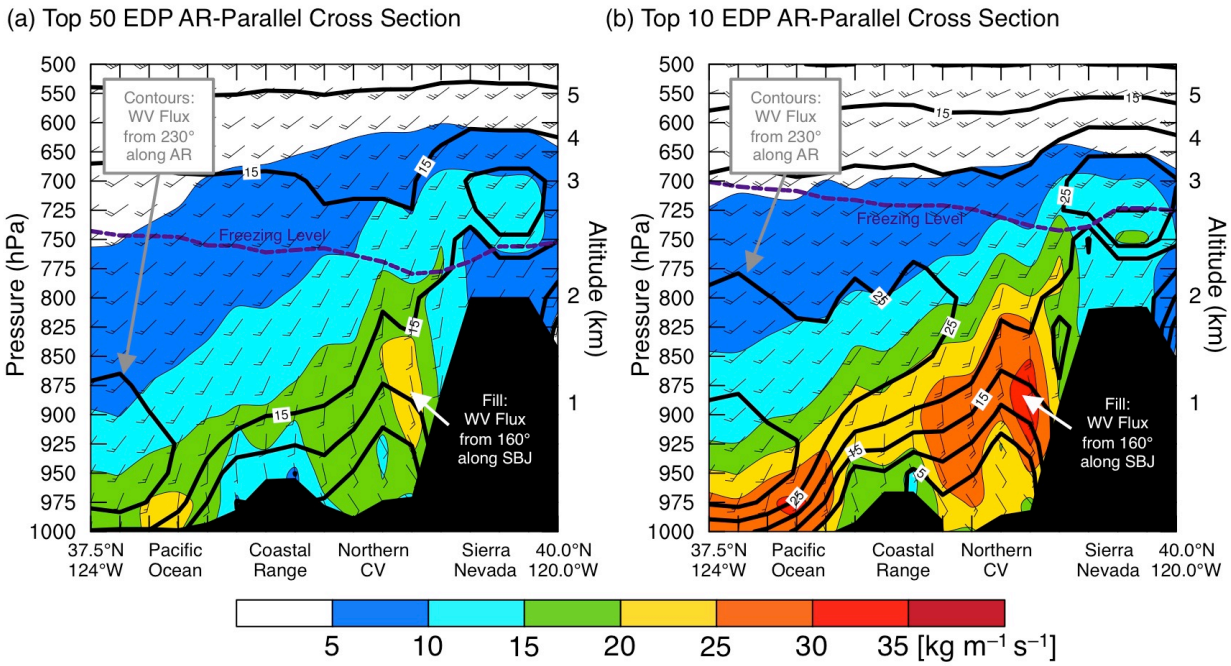

Fig. 4. Composite cross section along an AR-parellel line from 37.5°N, 124°W to 40°N, 120°W (shown in Fig. 3) of the (a) 50 days and (b) top-10 days with EDP that illustrates SBJ water vapor (WV) flux (kg m^{-1} s^{-1}; shaded according to scale), AR WV flux (contoured every 5 kg m^{-1} s^{-1} beginning at 5 kg m^{-1} s^{-1}) and total wind barbs (as in Fig. 2b). The SBJ WV flux is projection of total WV flux along 160°, whereas AR WV flux is projection of total WV flux along 230°.